ACS OMEGA

http://pubs.acs.org/journal/acsodf

Article

Highly Porous MIL-100(Fe) for the Hydrogen Evolution Reaction (HER) in Acidic and Basic Media

Ravi Nivetha, Kannan Gothandapani, Vimala Raghavan, George Jacob, Raja Sellappan, Preetam Bhardwaj, Sudhagar Pitchaimuthu, Arunachala Nadar Mada Kannan, Soon Kwan Jeong,* and Andrews Nirmala Grace*

Cite This: *ACS Omega* 2020, 5, 18941−18949

Read Online

ACCESS | Metrics & More | Article Recommendations | Supporting Information

ABSTRACT: The present study reports the synthesis of a porous Fe-based MOF named MIL-100(Fe) by a modified hydrothermal method without the HF process. The synthesis gave a high surface area with the specific surface area calculated to be 2551 $m^2\ g^{-1}$ and a pore volume of 1.407 $cm^3\ g^{-1}$ with an average pore size of 1.103 nm. The synthesized electrocatalyst having a high surface area is demonstrated as an excellent electrocatalyst for the hydrogen evolution reaction investigated in both acidic and alkaline media. As desired, the electrochemical results showed low Tafel slopes (53.59 and 56.65 mV dec^{-1}), high exchange current densities (76.44 and 72.75 mA cm^{-2}), low overpotentials (148.29 and 150.57 mV), and long-term stability in both media, respectively. The high activity is ascribed to the large surface area of the synthesized Fe-based metal−organic framework with porous nature.

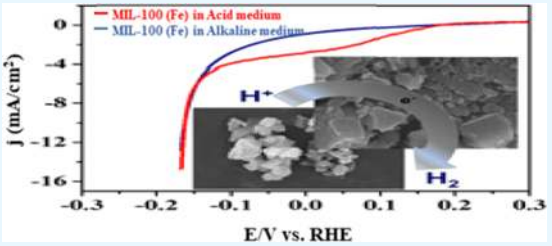

1. INTRODUCTION

It has become imperative to deal with economic needs and environmental pollutants affecting the globe due to the depletion of fossil fuels. Hydrogen is extensively investigated as an alternative fossil fuel and is considered as an eco-friendly gas carrier as a long-term option to reduce CO_2 emission as it is a clean, high-quality, and renewable energy resource.[1,2] Commonly, a large-scale H_2 production is accomplished by the gasification of coal and natural gas reforming, and the main concern for this is the use of nonrenewable energy and high temperature. Hence, among the various alternative processes, the electrochemical reduction method is considered to be effective to produce H_2 on a larger scale. The advantage of this hydrogen evolution reaction (HER) by electrochemical process is its simplicity and high stability.[3,4] A desirable cathodic H_2 reaction needs good electroactivity, stability, high surface area, and operability at a low potential. To reduce the overpotential of water electrolysis, the same is done by manipulation of the electrolyte and electrode materials. The HER delivers an active electrolyte (media) to meet future energy demands. An efficient electrocatalyst should help to endure the HER smoothly in both media (alkaline and acidic). The acidic medium enhances the proton transport rate, and the alkaline medium has less corrosion effect, thus allowing an extension of the choice of electrode materials.[5] Platinum is a well-known material for the HER, but its main drawbacks are high cost and tendency to get poisoned by chemicals like phosphate anions or sulfide, thus preventing its use.[6,7] Therefore, it is of utmost importance to construct a low-cost electrode with high electrocatalytic activity for the HER.[9]

Metal−organic frameworks, abbreviated as MOFs, are an important family of porous crystalline solids and have received significant interest in recent years in academia and industry. These materials are constructed by metal ions, and polyfunctional organic ligands possess excellent properties with high surface area, uniform tunable porosity, physicochemical properties, and attractive optical and electrical properties that have made them useful for several potential applications, viz., gas separation, organic molecule adsorption, gas storage, catalysis, biomimetic applications, drug delivery, magnetism, and optical devices.[8,10] Iron-based metal−organic frameworks are denoted as MIL-100(Fe) and are much researched among the various MOFs. The formation of MIL-100(Fe) via iron-building units is connected with 1,3,5-benzene tricarboxylic acid (BTC), and its molecular formula is $(Fe_3F(H_2O)_2O[C_6H_3(CO_2)_3]_2{\cdot}nH_2O)$.[11,12] Its powder X-ray diffraction (XRD) pattern indicates an octahedral cluster built by trimers of iron octahedra and BTC ligand (FeO_6) sharing a common vertex μ_3-O. MIL-100(Fe) have excellent qualities that distinguish them from other MOFs, such as biocompatibility, cost-effectiveness, permanent porosity, hydrothermal stability, relatively strong acid sites, water stability, and redox centers.[13,14] Ferey et al. have reported MIL-100(Fe) by the

Received: May 10, 2020
Accepted: June 30, 2020
Published: July 21, 2020

https://dx.doi.org/10.1021/acsomega.0c02171
ACS Omega 2020, 5, 18941−18949

hydrothermal method using HF and HNO_3 at 150 °C for 6 days, which gave a surface area of 2350.20 m^2 g^{-1}.[15] Moreover, HF acid is not eco-friendly, and in this view, zero-fluoride conditions have been successful in obtaining MIL-100(Fe). For instance, Zhang et al. have reported the synthesis of MIL-100(Fe) without the acid and achieved a surface area of 1836 m^2 g^{-1}.[16] Han et al. investigated the green route synthesis of MIL-100(Fe) similiarly and reported the corresponding value of 1940 m^2 g^{-1}.[17] MIL-100(Fe) was employed in various applications such as photocatalytic dye degradation, Fenton reaction, CO_2 absorption, heavy-metal removal, drug carrier, etc.,[18,19] as well as in electrocatalytic applications.[15] Sava Gillis and group validated the applicability of MIL-100(Fe) as electrocatalytic active anode electrodes for sodium-ion batteries,[20] which exhibited a high coulombic efficiency. Yamada et al. also demonstrated the same cathode electrodes for lithium-ion batteries, which exhibited a charge and discharge capacitance of 110 mAh g^{-1} and good thermal stability.[21] In this work, the green synthesis method was adopted to prepare MIL-100(Fe) using benzene tricarboxylic acid, iron(III) nitrate nonahydrate under HF-free hydrothermal conditions, and double-step purification process. The synthesized fluoride-free MOF showed a large surface area of 2551 m^2 g^{-1} with a pore volume of 1.4 mL g^{-1}, which favored the HER in both acidic and alkaline media. Results showed low Tafel slopes (53.59 and 56.65 mV dec^{-1}), high exchange current densities (76.44 and 72.75 mA cm^{-2}), low overpotentials (148.29 and 150.57 mV) in acidic and alkaline media, respectively, with long-term stability and good optical properties.

2. EXPERIMENTAL SECTION

2.1. Chemicals and Reagents. The reagents used in the work were of AR grade and used as received. Iron(III) nitrate nonahydrate ($Fe(NO_3)_3{\cdot}9H_2O$), trimesic acid (H_3BTC), and ethanol were procured from Aldrich. DI water from Milli-Q was used throughout this work.

2.2. Synthesis of MIL-100(Fe). The zero-fluoride catalyst was synthesized in accordance with the earlier reported method with slight modifications, as given in Scheme 1[22] In the procedure, 0.036 M $Fe(NO_3)_3{\cdot}9H_2O$ and 0.024 M H_3BTC-1,3,5-benzene tricarboxylic acid were blended and ground well to obtain a homogeneous mixture. The mixture was added to 36 mL of DI water, stirred, and later hydrothermally heated at 160 °C for 15 h. After the process, the material was dried after repeated centrifuging with warm DI water and ethanol, which was the first stage of purification. As a second step to nullify the residual substance, the acquired yellow powder dispersed in deionized water at 80 °C for 6 h was mixed with ethanol at 60 °C for 6 h. The highly purified product was dried at 150 °C for 6 h.

Scheme 1. Schematic of the Synthesis Procedure of MIL-100 (Fe) without HF Acid

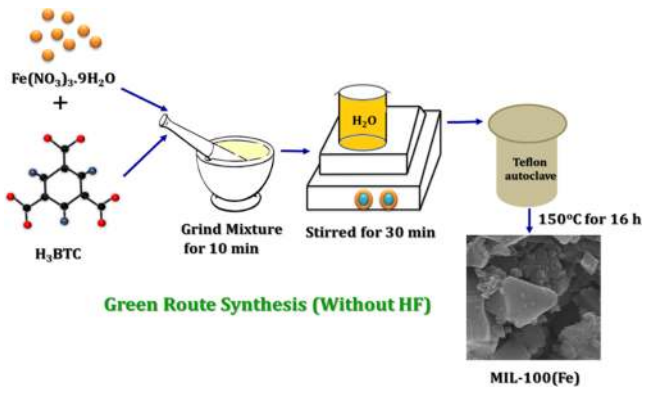

2.3. Reaction Mechanism in the Synthesis. Fe-based MOF was prepared using a hydrothermal method, and in general, it involves deprotonation of a Lewis acid ligand due to an increase in temperature and removal of a proton from the linker from its equilibrium due to precipitation followed by the LeChatelier principle. MIL-100(Fe) consists of μ_3-oxo-centered trimers of Fe(III) octahedral units, which is linked to six units of carboxylates and two H_2O molecules along with a hydroxyl anion group (Scheme 2) with a possible chemical formula of $Fe_3O(H_2O)_2(OH)0.19\{C_6H_3(CO_2)_3\}_2{\cdot}nH_2O$ (n = 14.5).[23] In the MIL-100(Fe)−water solvent system, where the iron nitrite is used as an iron source and 1,3,5-benzene tricarboxylic acid is used as a proton source (ligand), MIL-100(Fe) complexation of Fe^{3+} takes place with the formation of the water molecules complex, viz., $[Fe(H_2O)_5(OH)]^{2+}$ wherein the Fe^{3+} cation strongly complexes with water molecular reduction form hydroxide source.

Scheme 2. Schematic Showing the Structure Formation of MIL-100(Fe)

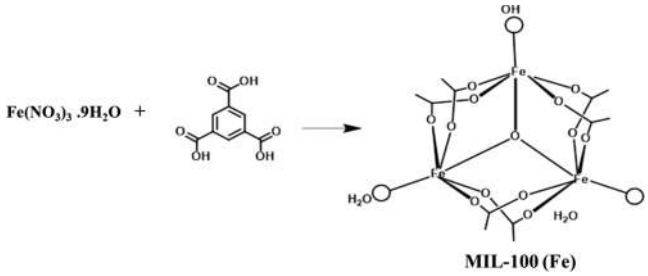

$$NO_3^- + H_2O \rightarrow NO_2^- + 2OH^- \quad (1)$$

$$NO_3^- + H_3BDC \rightarrow NO_2^- + H_2O + BDC^{(3-)} \quad (2)$$

$$NO_3^- + NO_2^- + 2H^+ \rightarrow 2NO_2 + H_2O \quad (3)$$

From eq 3, all absorbed protons slowly increase the pH level as desired for the formation of $[Fe_3(\mu_3\text{-}O)(H_2O)_2(OH)]$ units, hydroxide anions, and oxide along with deprotonation of H_3BTC. Hence, MIL-100(Fe) synthesis via the hydrothermal process using the said precursors in water molecules gave a high yield with large surface area due to the double-purification process.

2.4. Instrumentation. MIL-100(Fe) was analyzed with powder X-ray diffraction (XRD, Cu Kα D8 Advance, Bruker) to study the structural features and lattice arrangements. The morphological properties of the MOFs were studied by field emission scanning electron microscopy (FE-SEM- FEI Quanta 250 FEG) and transmission electron microscopy. The surface area, pore volume, and pore radius of the MOFs were analyzed by the BET analysis using a surface area analyzer (Quantachrome). The bonding between the metal and organic linkers was thoroughly studied by a Fourier transform infrared (FT-IR) spectrophotometer (Shimadzu) and a Raman spectrometer (Horbia Xplora Plus). The thermal stability of MIL-100(Fe) was investigated by thermogravimetry on a

https://dx.doi.org/10.1021/acsomega.0c02171
ACS Omega 2020, 5, 18941−18949

thermogravimetric analyzer (TA Instruments). All electrochemical measurements were performed at ambient temperature in an electrochemical workstation (CH Instruments) in a traditional three-electrode probe. A glassy carbon electrode with a geometric surface area of 1.766 mm^2 was used as the working electrode. It was polished well with an alumina kit (size: 0.05 μm), rinsed with deionized water, ultrasonicated in absolute ethanol, and dried at ambient temperature for a few minutes.

3. RESULTS AND DISCUSSION

3.1. Structural and Morphological Analysis. Structural analysis of the as-synthesized fluoride-free MOF was investigated by X-ray diffraction. As displayed in Figure 1,

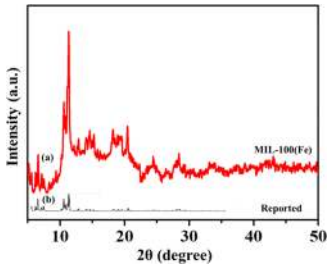

Figure 1. XRD spectrum of the (a) synthesized MIL-100(Fe) MOF and (b) that reported one in the literature.

the diffraction peak is in line with the simulated peaks.[24] The major peaks were seen at 5.65, 6.26, 10.58, 11.32, 12.22, 12.29, 14.60, 20.5, 24.5, and 28.3. Further, the morphology was investigated using SEM analysis and is given in Figure 2. The

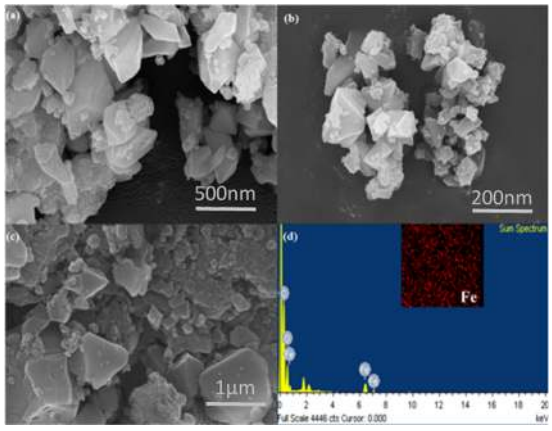

Figure 2. (a–c) SEM images of MIL-100(Fe) MOFs at various magnifications and (d) elemental analysis of MIL-100(Fe).

as-synthesized MIL-100(Fe) revealed an octahedral structure, and the EDAX analysis is given in Figure 2d. All of these results indicated that the formed MOFs are highly crystalline and are distributed homogeneously.

Further TEM images were taken and are given in Figure 3, and as seen from the images, the formed MIL-100(Fe) were irregular flakelike structures in accordance with the SEM results.

3.2. Elemental and Surface Analyses. To further confirm the embodiment of the MIL-100(Fe) structure, FT-IR spectrum was taken (Figure 4a). As observed from the figure, the band at 3370 cm^{-1} confirms the O–H stretching in

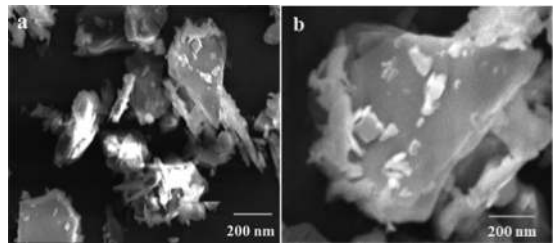

Figure 3. (a, b) TEM images of MIL-100(Fe) at different magnifications.

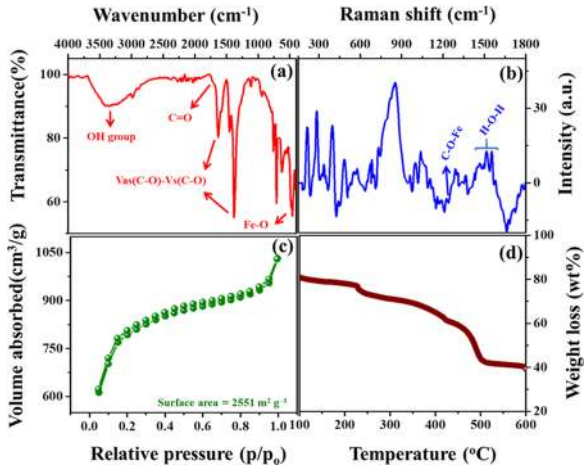

Figure 4. (a) FT-IR spectrum, (b) Raman spectrum, (c) N_2-adsorption and desorption isotherms, and (d) TGA curve of MIL-100(Fe).

the MOF due to the existence of H_2O moieties and the peak at 1726 cm^{-1} is due to the C═O stretching vibration in trimesic acid. Here, the H_3BTC peak is of low intensity due to the removal of the residual trimesic acid. The sharp band at 1630–1372 cm^{-1} is ascribed to the symmetric and asymmetric motions of the COO^- group. The 454 cm^{-1} peak corresponds to the Fe–O stretching vibration. These results confirm the structure of the formed MOF with trimesic acid–organic linker and metal ions (Fe).[25] Raman spectroscopy was further used to identify the structural information of the catalyst, as given in Figure 4b. In the 100–1900 cm^{-1} region, the band at 213 cm^{-1} can be associated with the Fe crystalline units, and the network binding and lattice vibration are seen from 450 to 600 cm^{-1}. The bands at 854 and 1000 cm^{-1} represent the aromaticity associated with the BTC group. The peak observed at 1200 cm^{-1} is due to the C–O–Fe of iron trimester, and those from 1400 to 1600 cm^{-1} are associated with H–OH bonding vibration due to metal node–organic linker (iron, trimesic acid) coordinated to the water molecules.[26] Thermogravimetric analysis is a useful tool to study the thermal stabilities of the sample. The synthesized MIL-100(Fe) show outstanding thermal stabilities up to 420 °C, as given in Figure 4d. From the three different stages of weight loss between 25 °C and 600 °C, the first weight loss of ∼20.98% from 25 to 100 °C corresponds to the dehydration happening inside the pores. The second weight loss of ∼27.64% from 100 to 250 °C is caused by H_2O molecules attached with the iron trimers. The final weight loss of 51.38% above 375 °C is assigned to the breakdown of the MOF, which resulted due to the disintegration of the organic linkers followed by the detriment of Fe species. Thus, experimental losses agree with the

https://dx.doi.org/10.1021/acsomega.0c02171
ACS Omega 2020, 5, 18941–18949

theoretical value according to the molecular formula, viz., $Fe_3O(H_2O)_2(OH)[C_6H_3(CO_2)_3]_2{\cdot}nH_2O$ ($n \sim 3.1$).[27] These results show the total thermal stability of the as-synthesized sample, which matched with the reported synthesis methods.[28] The textural properties of the as-synthesized fluoride-free sample were further analyzed by N_2 sorption and desorption isotherms at 77 K, as displayed in Figure 4c. The BET method was used to calculate the surface area to evaluate the structural, pore volume, pore size distribution, etc.; the BJH desorption method was also used (Figure 4c and Table 1). The specific surface area was calculated to be 2551 $m^2\ g^{-1}$ with pore volume and pore size calculated to be 1.407 $cm^3\ g^{-1}$ and 1.103 nm, respectively. The results are compared to the existing literature, as given in Table 1.

Table 1. Comparison of the Synthesized MIL-100(Fe) N_2 BET Isotherm Values with the Reported Ones

sample	synthesis process	BET surface area ($m^2\ g^{-1}$)	pore volume ($cm^3\ g^{-1}$)	reference
MIL-100(Fe)	hydrothermal without HF	1836	0.34	16
MIL-100(Fe)	hydrothermal with HF	1770	0.76	30
MIL-100(Fe)	microven method	1350	0.86	31
MIL-100(Fe)	hydrothermal HF, HNO_3	2350.20	-	32
MIL-100(Fe)/$CoFe_2O_4$	hydrothermal	2109	0.9	17
MIL-100	room temperature	2028	0.07	33
MIL-100	reflux	1593	0.88	34
MIL-100	hydrothermal HF, HNO_3	2546	-	35
MIL-100	green synthesis	1940	0.56	36
MIL-100	large-scale hydrothermal	1800	1.15	37
MIL-100	hydrothermal	1976	-	38
MIL-100	hydrothermal HNO_3, HF	2042	0.90	39
MIL-100	hydrothermal NH_4F	1626	-	40
MIL-100(Fe)	hydrothermal HF	2007	0.77	41
Au/MIL-100(Fe)	fabrication process	230	0.12	42
MIL-100(Fe)	hydrothermal	1598	-	43
MIL-100(Fe)	reflux HF, HNO_3	1754	0.80	44
MIL-100(Fe)	hydrothermal DMSO	1215	0.61	45
MIL-100(Fe)	hydrothermal, HF	1917	1.00	46
MIL-100(Fe)	hydrothermal without HF	2551	1.407	this work

In this comparison, the green route method of synthesis is successful, rendering the material with large surface area and making it catalytically more active higher than the reported materials (Table 1). Such increased values might be due to the increase in reaction time and the double-purification process. The catalyst exhibits type 1 isotherm according to the IUPAC classification, which indicates the microporous nature of the sample.[29] Thus, results show high surface and pore volume and hence could be an efficient catalyst for HER and photocatalytic applications.

3.3. Light Response and Stability Properties. UV−vis absorbance and reflectance spectra of the synthesized catalyst are given in Figure 5a,c, respectively, and the experiment was done to investigate its optical properties. MIL-100(Fe) exhibited an absorbance peak at 210 nm, attributed to the $\pi-\pi$ transitions of 1,3,5-benzene dicarboxylic ligand; furthermore, the broad absorbance peak observed at 320 nm is due to the ligand-to-metal charge-transfer (LMCT) signifying carboxylate oxygen moieties bond to metal ($^6A_{1g} \rightarrow {}^4A_{1g} + {}^4E_{g(G)}$) in Fe(III) or excitation process of Fe−O groups.[47] A small peak at 462 nm shows the strong visible light absorption. The Kubelka−Munk plot of $h\gamma$ is shown in Figure 5b, where the band gap E_g was calculated by the Tauq plot using the equation $K(h\gamma - E_g)^{1/n} = F(R)h\gamma$, where K represents the rate constant, $F(R)$ is the coefficient of absorption, and n is the optical transition. From the results, the band gap of MIL-100(Fe) was calculated to be 2.7 eV. Figure 5d demonstrates the photoluminescence (PL) spectra of MIL-100(Fe), where sample analysis was done at RT, excited at 320 nm, and the emission peak was observed at 475 nm. Mott−Schottky (MS) is a simple technique to examine the capacitance at the boundary of the semiconductor and electrolyte and carrier density. From the slope given in Figure 5b, the flat-band potential was calculated through the capacitance of the space charge layer measured at 1000 Hz ($1/C^2$2 vs V), as given by Mott−Schottky equation.[48]

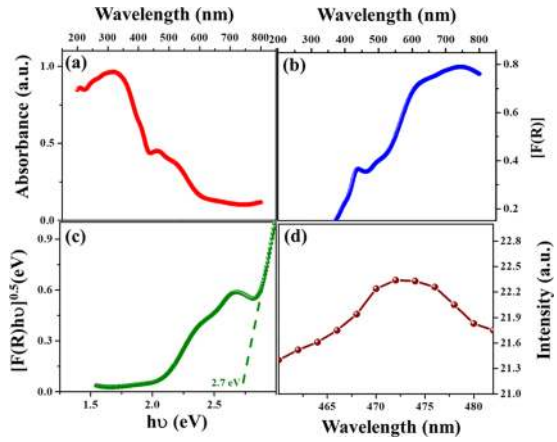

Figure 5. (a, c) UV spectrum absorbance and reflectance peaks of MIL-100(Fe); (b) Kubelka−Munk plot for MIL-100(Fe); and (d) photoluminescence study of MIL-100(Fe).

$$\frac{1}{C^2} = \frac{2}{\varepsilon e N d}$$

where C is the capacity per unit of space charge layer, e is the dielectric constant, ε_o is the vacuum permittivity, e is the charge of electron, Nd represents the concentration of the carrier, and k_B is the Boltzmann constant at absolute temperature T.

For MIL-100(Fe), the flat-band potential was determined to be −0.25 vs Ag/AgCl. The negative value indicates that the electron charge carrier (conduction band) is an N-type semiconductor. Figure 6a shows the transient photocurrent measurement under light, which is used to confirm the enhanced efficiency in the separation and transfer of charges in the on and off regions.[49] A photocurrent study of MIL-100(Fe) showed a high current value and thus a high charge

https://dx.doi.org/10.1021/acsomega.0c02171
ACS Omega 2020, 5, 18941−18949

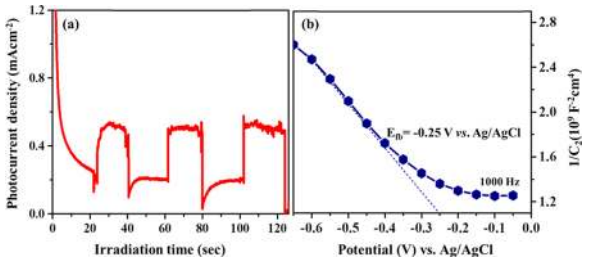

Figure 6. (a) Photocurrent study and (b) Mott−Schottky plots of the synthesized MIL-100(Fe) MOF.

separation efficiency of the photogenerated electron−hole pairs. ζ-Potential measurement helps us to understand the stability of the colloidal dispersions (Figure S1). To check the stability, the ζ-potential of the MOF was calculated to be −51.6 eV, with the conductivity value being 0.098 mS cm^{-1}.

3.4. HER Measurements. The HER activity was determined with a three-electrode configuration in both acidic and basic conditions using 0.5 M H_2SO_4 and 1 M NaOH, respectively, with a glassy carbon electrode (GC) (0.071 cm2) employed as the working electrode. The electrode was subjected to the standard cleaning protocols before experimentation in view of activating the surface. The electrodes were first electrochemically cycled between 0.1 and 0.4 V potentials to treat the surface. Further, 5 mg of the MIL-100(Fe) catalyst dissolved in 1 mL of ethanol was sonicated for 10 min. MIL-100(Fe) (5 μL) and Nafion (5 μL) were drop-cast onto the cleaned GC, and Pt and Ag/AgCl were used as auxiliary and reference probes, respectively. The mass loading of the catalyst was 1.77 μg cm^{-2}. The electrocatalytic property toward the hydrogen evolution reaction (HER) was examined using cyclic voltammetry at various scan rates (2, 20, 40, 60, 80, and 100 mV s^{-1}) in the nonfaradic region. The linear sweep voltammetry (LSV) technique is used to examine the onset potential, overpotential, current density, and Tafel slope. The Tafel slope is related to the exchange current density of the electrochemical reaction, and the kinetic mechanism is related to the rate-determining steps of the reaction. With respect to the hydrogen evolution reaction (HER), it is desirable to get a small value of the Tafel slope as this commonly reduces the overpotential needed to reach significant catalytic current densities.

3.4.1. Cyclic Voltammetry Studies for the HER. To enhance the electrocatalytic performance of MIL-100(Fe) in acidic and alkaline media toward the HER, the electrochemical surface area (ESCA) and electron transport are compared.[50] Thus, double-layer capacitance C_{dl} will give ESCA obtained from the cyclic voltammetry technique. The response of capacitance current from −0.2 to 0.4 V at various scan rates of 100−20 mV s^{-1} is given in Figure 7. According to McCrory's theory, the electrochemical double-layer capacitor (EDLC) shows the nature of the active electrochemical surface area of the solid−liquid interface.

All of the current measurements in the nonfaradic region were done by the CV analysis technique at various scan rates (Figure 7c,d). The double-layer capacitance values of MIL-100(Fe) in acidic and alkaline media were calculated to be 9.17 and 1.868 mF cm^{-1}, respectively, which shows that MIL-100(Fe) are electrochemically more active in the acidic medium.

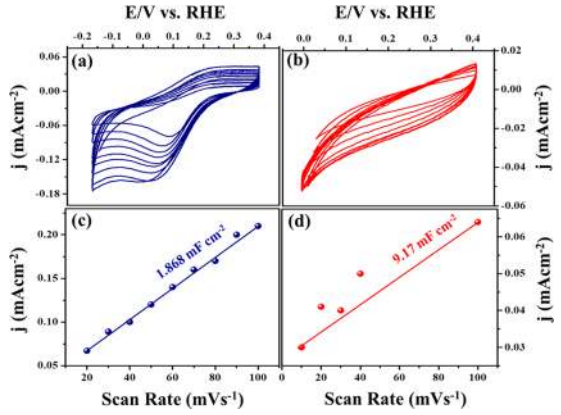

Figure 7. Cyclic voltammetry studies of MIL-100(Fe) in (a) alkaline medium and (b) acidic medium and the corresponding capacitance values of MIL-100(Fe) in (c) alkaline medium and (d) acidic medium.

3.4.2. Linear Sweep Voltammetry and Kinetics Studies for the HER. The linear sweep voltammetry technique is an efficient method to investigate the electrocatalytic activity of MIL-100(Fe) MOF in both acidic and alkaline media. The LSV peak of the material is given in Figure 8a, which shows

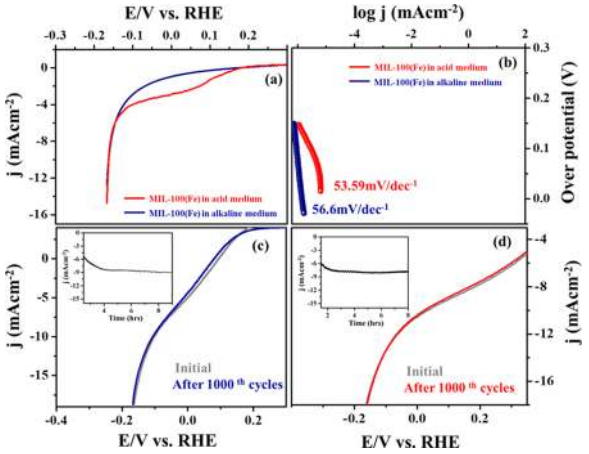

Figure 8. (a, b) Steady-state curves of polarization of MIL-100(Fe) and (c, d) cyclic stabilities of MIL-100(Fe) in 0.5 M H_2SO_4 and 1 M NaOH (the insets show the amperometric *i*−*t* curves of MIL-100(Fe) in alkaline and acidic media).

that the catalyst exhibited excellent performance with a low onset potential in acidic and alkaline media. The calculated onset potentials of MIL-100(Fe) in the acidic and alkaline media were calculated to be −0.07 and −0.084 V, respectively. Results show that the onset potential in alkaline medium was slightly higher than that in acidic medium solution, which might be due to the changes of electron transfer capability in different media.

3.5. Acidic Medium. The Tafel slope ($\log j$ (current density) vs overpotential) of the MIL-100(Fe) electrocatalyst in acidic medium was studied to achieve additional insight into the kinetic aspects and mechanism of HER activity. The slope of the MIL-100(Fe) catalyst derived from the linear portion of the plot is fit into the Tafel equation, viz., $\eta = a + b \log j$, where j is the current density, η represents the overpotential, and b is the corresponding Tafel slope (Figure 8b). The exchange current density, also given by j_o, can be accessed by the

https://dx.doi.org/10.1021/acsomega.0c02171
ACS Omega 2020, 5, 18941−18949

intrinsic rate electron transfer via extrapolation.[51] The value j_o was calculated to be 76.44 mA cm^{-2} with an overpotential of 150.57 mV. In general, three major steps are regarded for converting H^+ to H_2 toward the HER in acidic medium commonly termed the Volmer, Heyrovsky, and Tafel process, corresponding to a proton electrosorption (eq 4), desorption via electrochemical represents (eq 5), and the surface-adsorbed hydrogen recombination (eq 6) to the initial absorption of protons from acid solution to form absorbed ($H \rightarrow H_{ad}$) and generally regarded as the fast reaction. When the slope value is 120 mV dec^{-1}, the Heyvosky and Tafel reactions are stated as two primary reactions for H_2 evolution. The Heyvosky reaction is an electrochemical desorption process with a slope of 40 mV dec^{-1}, and finally, the Tafel reaction is the RDS with a value of 30 mV dec^{-1}.[52]

$$H_2O + \text{catalyst} + e^- \rightarrow \text{catalyst} - H^* + OH^- \quad (4)$$

$$H^+ + e^- + H_{ad} \rightarrow H_2 \quad (5)$$

$$H_{ad} + H_{ad} + \rightarrow H_2 \quad (6)$$

where other reactions are the Volmer–Heyrovsky reaction and the Volmer–Tafel mechanism possible for the HER. In the former, the solvated proton from the water layer interacts with one absorbed surface hydrogen to get converted to H_2 (eq 5), and the absorbed surface hydrogen in the vicinity interacts to form molecular H_2 known as the Volmer–Tafel mechanism given in eq 3.[53] Accordingly, the observed Tafel slope range was calculated to be 53.59 mV dec^{-1}. For HER electrocatalysis using MIL-100(Fe), the value of α is 0.5 and hence the HER is controlled by the Volmer–Heyrovsky reaction (Table 2).

Table 2. Tafel Slope and Exchange Current Density Values Calculated for the HER Using MIL-100(Fe)

S. No.	catalyst	$-\log j_o$ (mA cm^{-2})	b (mV dec^{-1})	α
1	MIL-100(Fe) in acidic medium	76.44	53.59	1.05
2	MIL-100(Fe) in alkaline medium	72.75	56.65 mV	1.11

3.6. Alkaline Medium. The Tafel slope ($\log j$ (current density) vs overpotential) of the MIL-100(Fe) electrocatalyst in alkaline medium was further explored to achieve added insights into the kinetic mechanism of the HER. The Tafel slopes of the MIL-100(Fe) catalysts are obtained from the linear part of the plot, which was further fitted in the Tafel equation $\eta = a + b \log j$ (Figure 8b). The exchange current density (j_o) due to the intrinsic rate electron transfer is calculated via extrapolation of the basic Tafel equation;[54] the value of J_o was calculated to be 72.75 mA cm^{-2} with an overpotential of 148.29 mV. In general, there are three major ways for the conversion of H^+ to H_2 in alkaline medium, viz., Volmer, Heyvosky, and Tafel reactions. Volmer gives the proton discharge electrosorption (eq 7), electrochemical desorption is the Heyvosky reaction (eq 8), and finally, Tafel represents the recombination of two surface-absorbed H_2 atoms (eq 9).[55]

$$M + H_3O^+ + e^- \rightarrow MH_{ads} + H_2O \quad (b \sim 120 \text{ mV}) \quad (7)$$

$$MH_{ads} + MH_{ads} \rightarrow M + H_2 \quad (b \sim 40 \text{ mV}) \quad (8)$$

$$MH_{ads} + H_3O^+ + e \rightarrow 2M + H_2 + H_2 + H_2O \ (b \sim 30 \text{ mV}) \quad (9)$$

where MH_{ads} is the H_2 atom absorbed and M signifies the active free sites available for HER. From the results, the slope was calculated to be 56.65 mV dec^{-1}, from which it is suggested that the electrodesorption reaction becomes a rate-limiting step also designated as the Volmer–Heyvosky reaction, as given in Table 2. Hence, the MIL-100(Fe) electrocatalyst in both media exhibits a high exchange current density j_o, a low onset potential along with a low Tafel slope, and a low overpotential suggesting that MIL-100(Fe) is an effective material for the HER. To further emphasize the importance of the catalyst materials, a table of comparison is given in Table S1, from which it is evident that the prepared MOF shows enhanced electrocatalytic activity of the HER. The catalyst stability test was further evaluated under acidic and alkaline conditions by a long-term cyclic stability test.

The long-term HER stability was verified by the chronoamperometric i–t technique for 8 h in 1 M NaOH and 0.5 M H_2SO_4 (insets in Figure 8c,d). As observed from the tests, it was quite stable without much shift in the current density. Results show a stable HER catalytic performance with negligible degradation even after 1000 cycles and that the current density is nearly constant during the continuous operation for 8 h. The polarization curves measured before and after 1000 cycles had no significant changes in acidic medium, whereas in alkaline medium, a slight difference in current density was observed due to the H^+ or H_2 bubbles observed on the electrode, which further impedes the reaction. Thus, the results show that the MIL-100(Fe) catalyst is highly active and stable in both media.

To assess the kinetic charge transport (electrode/electrolyte interface study), it was characterized by electrochemical impedance spectroscopy measurement with a three-electrode probe.[56] A small semicircle is attributed to the charge transfer near the user interface of the HER (Figure 9a,b). The Nyquist plot of MIL-100 (Fe) was constructed in acidic and alkaline media at an applied voltage of 0.39 V and frequency of 0.1–10^5 Hz. The R_{ct} value of the MOF material in the alkaline medium was calculated to be 8.71 Ω, and 8.04 Ω in the acidic medium. The low resistance in the acidic medium could be related to the higher charge transport of the HER in acidic medium. Hence, MIL-100 (Fe) in alkaline and acidic media show more efficient charge transport for the HER activity.

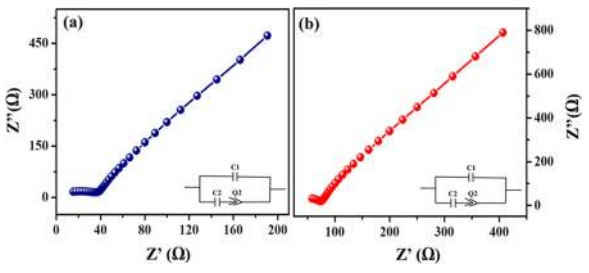

Figure 9. Nyquist plot of the MIL-100(Fe) electrode observed at an amplitude of 200 mV and frequency range of 0.1 Hz to 0.1 MHz in (a) alkaline medium and (b) acidic medium. The insets show equivalent circuit of the MIL-100(Fe) electrode.

https://dx.doi.org/10.1021/acsomega.0c02171
ACS Omega 2020, 5, 18941–18949

4. CONCLUSIONS

Highly porous MIL-100(Fe) with large surface areas were successfully prepared by the hydrothermal method (without HF) and further tested toward the HER. The synthesized electrocatalyst exhibited excellent activity toward the HER in acidic and alkaline media. Electrochemical results show low Tafel slopes (53.59 and 56.65 mV dec^{-1}), large exchange current densities (76.44 and 72.75 mA cm^{-2}), low overpotentials (148.29 and 150.57 mV), and good stability in both acidic and basic media, respectively. This high electrocatalytic activity of the HER could be due to the high surface area with porous nature and homogeneous morphology. Results thus show that the synthesized catalyst could be used as an HER electrocatalyst, and in view of its excellent surface area, the MOF could be used for other catalytic applications.

■ ASSOCIATED CONTENT

Supporting Information

The Supporting Information is available free of charge at https://pubs.acs.org/doi/10.1021/acsomega.0c02171.

ζ-Potential measurement of MIL-100(Fe) (Figure S1) and comparison of the electrocatalyst MOF with the reported ones (Table S1) (PDF)

■ AUTHOR INFORMATION

Corresponding Authors

Soon Kwan Jeong − *Climate Change Technology Research Division, Korea Institute of Energy Research, Daejeon 305-343, South Korea;* orcid.org/0000-0001-5347-3651; Email: jeongsk@kier.re.kr

Andrews Nirmala Grace − *Centre for Nanotechnology Research, VIT University, Vellore 632014, India;* orcid.org/0000-0002-2016-3013; Email: anirmalagrace@vit.ac.in, anirmalaglady s@gmail.com

Authors

Ravi Nivetha − *Centre for Nanotechnology Research, VIT University, Vellore 632014, India*

Kannan Gothandapani − *Centre for Nanotechnology Research, VIT University, Vellore 632014, India*

Vimala Raghavan − *Centre for Nanotechnology Research, VIT University, Vellore 632014, India*

George Jacob − *Centre for Nanotechnology Research, VIT University, Vellore 632014, India*

Raja Sellappan − *Centre for Nanotechnology Research, VIT University, Vellore 632014, India*

Preetam Bhardwaj − *Centre for Nanotechnology Research, VIT University, Vellore 632014, India*

Sudhagar Pitchaimuthu − *Photocatalyst and Coatings Group, SPECIFIC, College of Engineering, Swansea University (Bay Campus), Swansea SA1 8EN, U.K.*

Arunachala Nadar Mada Kannan − *Ira A. Fulton Schools of Engineering, Arizona State University, Mesa, Arizona 85212, United States;* orcid.org/0000-0002-8412-1680

Complete contact information is available at: https://pubs.acs.org/10.1021/acsomega.0c02171

Notes

The authors declare no competing financial interest.

■ REFERENCES

(1) Omer, A. M. Identifying, developing, and moving sustainable communities through application of bioenergy for energy or materials: future perspective through energy efficiency. *Int. J. Life Sci.* **2017**, *1*, 8−34.

(2) Momirlan, M.; Veziroglu, N. The properties of hydrogen as fuel tomorrow in sustainable energy system for a cleaner planet. *Int. J. Hydrogen Energy* **2005**, *30*, 795−802.

(3) Geng, S.; Hu, L.; Weiwei, Y.; Yong, S. Y. Activating the MoS_2 Basal Plane by Controllable Fabrication of Pores for an Enhanced Hydrogen Evolution Reaction. *Chem. - Eur. J.* **2018**, *24*, 19075−19080.

(4) Logan, B. E.; Douglas, C.; Shaoan, C.; Hubertus, H.; Tom, S.; Adriaan, W. J.; Rene, R. Microbial electrolysis cells for high yield hydrogen gas production from organic matter. *Environ. Sci. Technol.* **2008**, *42*, 8630−8640.

(5) Geng, S.; Weiwei, Y.; Yong, S. Y. Building MoS2/S-doped g-C_3N_4 layered heterojunction electrocatalysts for efficient hydrogen evolution reaction. *J. Catal.* **2019**, *375*, 441−447.

(6) Gómez, M. J.; Loia′cono, A.; Pe′rez, L. A.; Franceschini, E. A.; Lacconi, G. I. Highly Efficient Hybrid Ni/Nitrogenated Graphene Electrocatalysts for Hydrogen Evolution Reaction. *ACS Omega* **2019**, *4*, 2206−2216.

(7) Ling, Y.; Luo, F.; Zhang, Q.; Qu, K.; Guo, L.; Hu, H.; Yang, Z.; Cai, W.; Cheng, H. Tungsten Carbide Hollow Microspheres with Robust and Stable Electrocatalytic Activity toward Hydrogen Evolution Reaction. *ACS Omega* **2019**, *4*, 4185−4191.

(8) Geng, S.; Yequn, L.; Yong, S. Y.; Weiwei, Y.; Haibo, L. Engineering defects and adjusting electronic structure on S doped MoO_2 nanosheets toward highly active hydrogen evolution reaction. *Nano Res.* **2020**, *13*, 121−126.

(9) Nayak, A. K.; Verma, M.; Sohn, Y.; Deshpande, P. A.; Pradhan, D. Highly active tungsten oxide nanoplate electrocatalysts for the hydrogen evolution reaction in acidic and near neutral electrolytes. *ACS Omega* **2017**, *2*, 7039−7047.

(10) Pan, S.; Kong, X.; Zhang, Q.; Xu, Q.; Wang, M.; Wei, C.; Zhao, Y.; Zhang, X. Rational modulating electronegativity of substituents in amorphous metal-organic frameworks for water oxidation catalysis. *Int. J. Hydrogen Energy* **2020**, *45*, 9723−9732.

(11) Ferrando-Soria, J.; Hossein, K.; Pablo, C.; Jorge, G.; Freek, K.; Miguel, J.; Francesc, L.; et al. Highly selective chemical sensing in a luminescent nanoporous magnet. *Adv. Mater.* **2012**, *24*, 5625−5629.

(12) Xie, L.; Dahuan, L.; Hongliang, H.; Qingyuan, Y.; Chongli, Z. Efficient capture of nitrobenzene from waste water using metal−organic frameworks. *Chem. Eng. J.* **2014**, *246*, 142−149.

(13) Chinnappan, A.; Dongxiao, J.; Chinnappan, B.; Xiaohong, Q.; Seeram, R.; Jayathilaka, W. A. D. M. Facile synthesis of electrospun C@ NiO/Ni nanofibers as an electrocatalyst for hydrogen evolution reaction. *Int. J. Hydrogen Energy* **2018**, *43*, 15217−15224.

(14) Yoon, J. W.; You, S.; Young, H.; Jong, C.; Herve, L.; Stefan, W.; et al. Philippe Controlled reducibility of a metal−organic framework with coordinatively unsaturated sites for preferential gas sorption. *Angew. Chem., Int. Ed.* **2010**, *49*, 5949−5952.

(15) Horcajada, P.; Surblé, S.; Serre, C.; Hong, D.-Y.; Seo, Y.-K.; Chang, J.-S.; Grenèche, J.-M.; Margiolaki, I.; Férey, G. Synthesis and catalytic properties of MIL-100 (Fe), an iron (III) carboxylate with large pores. *Chem. Commun.* **2007**, *27*, 2820−2822.

(16) Zhang, F.; Shi, J.; Jin, Y.; Fu, Y.; Zhong, Y.; Zhu, W. Facile synthesis of MIL-100 (Fe) under HF-free conditions and its application in the acetalization of aldehydes with diols. *Chem. Eng. J.* **2015**, *259*, 183−190.

(17) Han, L.; Qi, H.; Zhang, D.; Ye, G.; Zhou, W.; Hou, C.; Xu, W.; Sun, Y. A facile and green synthesis of MIL-100 (Fe) with high-yield and its catalytic performance. *New J. Chem.* **2017**, *41*, 13504−13509.

(18) Dhakshinamoorthy, A.; Mercedes, A.; Patricia, H.; Emma, G.; Muthusamy, V.; Alexandre, V.; Jean, G.; Christian, S.; Marco, D.; Hermenegildo, G. Comparison of porous iron trimesate Basolite F300 and MIL-100 (Fe) as heterogeneous catalysts for Lewis acid and

oxidation reactions: roles of structural defects and stability. *ACS Catal.* **2012**, *2*, 2060−2065.
(19) Čelič, T. B.; Rangus, M.; Lázár, K.; Kaučič, V.; Natasa, Z. L. Spectroscopic Evidence for the Structure Directing Role of the Solvent in the Synthesis of Two Iron Carboxylates. *Angew. Chem., Int. Ed.* **2012**, *51*, 12490−12494.
(20) Wang, D.; Renkun, H.; Wenjun, L.; Dengrong, S.; Zhaohui, L. Fe-based MOFs for photocatalytic CO_2 reduction: role of coordination unsaturated sites and dual excitation pathways. *ACS Catal.* **2014**, *4*, 4254−4260.
(21) Yamada, T.; Shiraishi, K.; Kitagawa, H.; Kimizuka, N. Applicability of MIL-101 (Fe) as a cathode of lithium ion batteries. *Chem. Commun.* **2017**, *53*, 8215−8218.
(22) Huang, S.; Yang, K.-L.; Liu, X.-F.; Pan, H.; Zhang, H.; Yang, S. MIL-100(Fe)-catalyzed efficient conversion of hexoses to lactic acid. *RSC Adv.* **2017**, *7*, 5621−5627.
(23) Sahai, S.; Ashi, I.; Snigdha, R.; Rohit, S.; Sahab, D.; Vibha, R. S. Augmented photoelectrochemical response of CdS/ZnS quantum dots sensitized hematite photoelectrode. *Int. J. Energy Res.* **2016**, *40*, 1811−1819.
(24) Sarangi, S. N.; Adhikari, P. K.; Sahu, S. N.; Pandey, D. Current−voltage and capacitance−voltage studies of nanocrystalline CdSe/Au Schottky junction interface. *J. Nanopart. Res.* **2010**, *12*, 2277−2286.
(25) Watanabe, M. Dye-sensitized photocatalyst for effective water splitting catalyst. *Sci. Technol. Adv. Mater.* **2017**, *18*, 705−723.
(26) Canioni, R.; Catherine, M.; Francis, S.; Patricia, H.; Christian, S.; Menaschi, H.; Gerard, F.; et al. Stable polyoxometalate insertion within the mesoporous metal organic framework MIL-100 (Fe). *J. Mater. Chem.* **2011**, *21*, 1226−1233.
(27) Jin, Y.; Shi, Z.; Zhong, Y.; Zhu, W.; Zhang, F. Synthesis of sulfonic acid-functionalized MIL-101 for acetalization of aldehydes with diols. *J. Mol. Catal. A: Chem.* **2014**, *383*−*384*, 167−171.
(28) Li, X.; Lachmanski, S.; Safi, S.; Sene, C.; Serre, G.; Zhang, J.; Gref, R.; Grenèche, J. M. New insights into the degradation mechanism of metal-organic frameworks drug carriers. *Sci. Rep.* **2017**, No. 13142.
(29) Leofanti, G.; Padovan, M.; Venturelli, B.; Tozzola, G. Surface area and pore texture of catalysts. *Catal. Today* **1998**, *41*, 207−219.
(30) Peng, J.; Sikai, X.; Jing, X.; Yan, H.; Qibin, X.; Haihui, W.; Zhong, L. A supported Cu (I)@ MIL-100 (Fe) adsorbent with high CO adsorption capacity and CO/N_2 selectivity. *Chem. Eng. J.* **2015**, *270*, 282−289.
(31) Yang, C.-X.; Chang, L.; Yi, C.; Xiu, Y. Metal−organic framework MIL-100 (Fe) for artificial kidney application. *RSC Adv.* **2014**, *4*, 40824−40827.
(32) Seo, Y.-K.; Yoon, J. W.; Lee, J. S.; Lee, U.-H.; Hwang, Y. K.; Jun, C. H.; Horcajada, P.; Serre, C.; Chang, J.-S. Large scale fluorine-free synthesis of hierarchically porous iron (III) trimesate MIL-100 (Fe) with a zeolite MTN topology. *Microporous Mesoporous Mater.* **2012**, *157*, 137−145.
(33) Guesh, K.; Clarice, C.; Alvaro, M.; Manuel, G.; Isabel, D.; Manuel, S. Sustainable preparation of MIL-100 (Fe) and its photocatalytic behavior in the degradation of methyl orange in water. *Cryst. Growth Des.* **2017**, *17*, 1806−1813.
(34) Shi, J.; Shengtao, H.; Huanhuan, L.; Yanghe, F.; Fumin, Z.; Yijun, Z.; Weidong, Z. Synthesis of MIL-100 (Fe) at low temperature and atmospheric pressure. *J. Chem.* **2013**, No. 792827.
(35) Liang, R.; Fenfen, J.; Lijuan, S.; Na, Q.; Ling, W. M @ MIL-100 (Fe)(M = Au, Pd, Pt) nanocomposites fabricated by a facile photo deposition process: Efficient visible-light photocatalysts for redox reactions in water. *Nano Res.* **2015**, *8*, 3237−3249.
(36) Ke, F.; Junfa, Z.; Ling, Q.; Xia, J. Controlled synthesis of novel Au@ MIL-100 (Fe) core−shell nanoparticles with enhanced catalytic performance. *Chem. Commun.* **2013**, *49*, 1267−1269.
(37) Dhakshinamoorthy, A.; Mercedes, A.; Young, H.; You, S.; Avelino, C.; Hermenegildo, G. Intracrystalline diffusion in Metal Organic Framework during heterogeneous catalysis: Influence of particle size on the activity of MIL-100 (Fe) for oxidation reactions. *Dalton Trans.* **2011**, *40*, 10719−10724.
(38) Bezverkhyy, I.; Weber, G.; Bellat, J. P. Degradation of fluoride-free MIL-100 (Fe) and MIL-53 (Fe) in water: Effect of temperature and pH. *Microporous Mesoporous Mater.* **2016**, *219*, 117−124.
(39) Yang, J.-C.; Xue, X.-B. $CoFe_2O_4$@ MIL-100 (Fe) hybrid magnetic nanoparticles exhibit fast and selective adsorption of arsenic with high adsorption capacity. *Sci. Rep.* **2017**, *7*, No. 40955.
(40) Jeremias, F.; Stefan, H.; Christoph, J. Ambient pressure synthesis of MIL-100 (Fe) MOF from homogeneous solution using a redox pathway. *Dalton Trans.* **2016**, *45*, 8637−8644.
(41) Xie, Q.; Yan, L.; Zhaoling, L.; Hang, Z.; Xiangjun, Y.; Jing, C.; Hong, G. Effective adsorption and removal of phosphate from aqueous solutions and eutrophic water by Fe-based MOFs of MIL-101. *Sci. Rep.* **2017**, No. 3316.
(42) Huo, S.; Xiu, Y. Metal−organic framework MIL-100 (Fe) for the adsorption of malachite green from aqueous solution. *J. Mater. Chem.* **2012**, *22*, 7449−7455.
(43) Yang, J.; Xiaojun, N.; Shaorong, A.; Weiyi, C.; Jie, W.; Wei, L. Facile synthesis of Bi_2 MoO 6−MIL-100 (Fe) metal−organic framework composites with enhanced photocatalytic performance. *RSC Adv.* **2017**, *7*, 2943−2952.
(44) Liang, R.; Shuiguang, L.; Fenfen, J.; Lijuan, S.; Na, Q.; Ling, W. A simple strategy for fabrication of Pd@ MIL-100 (Fe) nanocomposite as a visible-light-driven photocatalyst for the treatment of pharmaceuticals and personal care products (PPCPs). *Appl. Catal., B* **2015**, *176*−*177*, 240−248.
(45) Liu, X.; Rui, D.; Wenjun, D.; Xiubing, H.; Jia, T.; Hongyi, G.; Ge, W. A sandwich-like heterostructure of TiO_2 nanosheets with MIL-100 (Fe): A platform for efficient visible-light-driven photocatalysis. *Appl. Catal., B* **2017**, *209*, 506−513.
(46) Reinsch, H.; Norbert, S. Formation and characterisation of Mn-MIL-100. *Cryst. Eng. Comm.* **2013**, *15*, 544−550.
(47) Tan, F.; Min, L.; Keyan, L.; Yiren, W.; Junhu, W.; Xinwen, G.; Guoliang, Z.; Chunshan, S. Facile synthesis of size-controlled MIL-100 (Fe) with excellent adsorption capacity for methylene blue. *Chem. Eng. J.* **2015**, *281*, 360−367.
(48) Dhakshinamoorthy, A.; Mercedes, A.; Young, K. H.; You-Kyong, S.; Avelino, C.; Hermenegildo, G. Intracrystalline diffusion in Metal Organic Framework during heterogeneous catalysis: Influence of particle size on the activity of MIL-100 (Fe) for oxidation reactions. *Dalton Trans.* **2011**, *40*, 10719−10724.
(49) Zhang, S.; Lina, L.; Sangen, Z.; Zhihua, S.; Junhua, L. Construction of interpenetrated ruthenium metal−organic frameworks as stable photocatalysts for CO_2 reduction. *Inorg. Chem.* **2015**, *54*, 8375−8379.
(50) Li, X.-H.; Markus, A. Metal nanoparticles at mesoporous N-doped carbons and carbon nitrides: functional Mott−Schottky heterojunctions for catalysis. *Chem. Soc. Rev.* **2013**, *42*, 6593−6604.
(51) Li, M.; Mingchuan, L.; Zhonghong, X.; Yong, Y.; Yarong, H.; Dong, W.; Yingjun, S.; et al. Modulating the surface segregation of PdCuRu nanocrystals for enhanced all-pH hydrogen evolution electrocatalysis. *J. Mater. Chem. A* **2019**, *7*, 20151−20157.
(52) Fan, K.; Hong, C.; Yongfei, J.; Hui, H.; Claesson, P. M.; Daniel, Q.; Philippe, B.; et al. Nickel−vanadium monolayer double hydroxide for efficient electrochemical water oxidation. *Nat. Commun.* **2016**, *7*, No. 11981.
(53) Shi, Z.; Kaiqi, N.; Zheng, S.; Boxu, G.; Huanlei, L.; Hongbin, Z.; Bolun, L.; et al. Phosphorus-Mo_2 C @ carbon nanowires toward efficient electrochemical hydrogen evolution: composition, structural and electronic regulation. *Energy Environ. Sci.* **2017**, *10*, 1262−1271.
(54) Yu, X.-Y.; Feng, Y.; Jeon, Y.; Guan, B.; Lou, X. W. D.; Paik, U. Formation of Ni−Co−MoS_2n nanoboxes with enhanced electrocatalytic activity for hydrogen evolution. *Adv. Mater.* **2016**, *28*, 9006−9011.
(55) Tang, Y. J.; Gao, M.-R.; Liu, C. H.; Li, S.-L.; Jiang, H.-L.; Lan, Y.-Q.; Han, M.; Yu, S.-H. Porous molybdenum-based hybrid catalysts for highly efficient hydrogen evolution. *Angew. Chem., Int. Ed.* **2015**, *54*, 12928−12932.

https://dx.doi.org/10.1021/acsomega.0c02171
ACS Omega 2020, 5, 18941−18949

(56) Kaninski, M. P. M.; Nikolić, V. M.; Potkonjak, T. N.; Simonović, B. R.; Potkonjak, N. I. Catalytic activity of Pt-based intermetallic for the hydrogen production—Influence of ionic activator. *Appl. Catal., A* **2007**, *321*, 93−99.

https://dx.doi.org/10.1021/acsomega.0c02171
ACS Omega 2020, 5, 18941−18949